Investigation of Micro-Capillary Plates to Enhance Low-Frequency Sound Absorption

Cédric Maury, Teresa Bravo

INVESTIGATION OF MICRO-CAPILLARY PLATES TO ENHANCE LOW-FREQUENCY SOUND ABSORPTION

Cédric Maury[1] **Teresa Bravo[2]**
[1] Aix-Marseille Univ., CNRS, Centrale Marseille, Laboratoire de Mécanique et d'Acoustique (LMA), 4, impasse Nikola Tesla, 13013 Marseille, France
[2] Consejo Superior de Investigaciones Cientificas (CSIC), ITEFI-CSIC, Serrano 144, 28006, Madrid, Spain
cedric.maury@centrale-marseille.fr

ABSTRACT

Theoretical, numerical and experimental studies are presented that investigate the wideband absorption properties of unbacked and rigidly-backed micro-capillary plates (MCPs) under normal plane wave incidence. MCPs are characterized by a perforation ratio greater than 50 % and channels diameters between 4μm and 50μm, thus leading to a thin porous absorber with a regular distribution of at most one million of micro-channels per cm^2. They are fabricated by micro-chemical etching process. Unlike micro-perforated panels, the MCPs have a high perforation ratio that ensures minute reactance, thereby reducing their transfer impedance to a pure resistance over a broad frequency range. Moreover, their micrometric channels diameter allows tailoring their resistance to achieve constant target absorption over a wide frequency band. This property has been validated through finite-element simulations that also confirmed isothermal conditions in capillary channels. An optimal value of the micro-channels diameter can be derived that achieves maximal viscous dissipation of the acoustical energy under plane wave anechoic load. Kundt tube experiments confirmed the ability of optimized MCPs to achieve wideband flat absorption performance that exceeds 0.85 up to a Helmholtz number of 0.3. They also showed the potential of non-optimal acoustically-transparent MCPs to achieve a low-frequency anechoic termination.

1. INTRODUCTION

The attenuation of the acoustic pressure field is still a challenging task when addressing the control of low frequency components. Passive methods can provide significant noise reduction, but also additional weight and size to the control device.

Micro-Perforated Panels (MPP) are alternative solutions for situations when porous components are excluded due, for instance, to the presence of a mean flow. Typical MPPs are composed of a panel with sub-millimetric holes backed by a cavity. The physical parameters defining the acoustic properties of the screen are the thickness, the size of the perforation and the perforation ratio or porosity [1,2]. The backing cavity depth has to be chosen to build the Helmholtz-type resonance. Although many works have been restricted to the study of infinite layer considering only the absorption performance of these materials, a more complete description has been developed in recent years considering the finite dimensions of the partitions, their vibrating response [3] and their transmission properties [4]. To avoid limitations concerning the size of the whole device, multi-layered MPPAs, combining several parallel MPPs and cavities, filled also with porous material, have been considered [5]. Their wideband absorption performance is then due to cross-coupling mechanisms between the partition resonators.

Of interest is to downshift the first Helmholtz-type resonance without increasing the cavity depth. This can be achieved by partitioning the cavity in individual cells centered on the axis of the apertures and by increasing the acoustic path length in the cell cavities, for instance by inserting a rectangular coil in the cross-sectional plane of the cavities [6]. Such device has an overall height equal to that of a rigidly-backed MPP. Given the cavity width and depth, a target acoustic path length can be determined by a suitable choice of the inner walls thickness, of their separation distance and of the number of folding turns in the coiled resonators in order to achieve low-frequency absorption, albeit narrow-band. In all cases, a causality constraint has been derived [7], that reveals a trade-off between the relative absorption bandwidth and the absorbent overall thickness.

In practice, most of the studies concerning rigidly-backed MPPs consider perforations with characteristic diameters usually greater than 0.2 mm and with low perforation ratio, that provide half-absorption bandwidth lower than two octaves at the Helmholtz resonance. To broaden the bandwidth beyond two octaves, the apertures should be diminished down to the range 100 – 200 μm, increasing the manufacturing cost procedure.

The goal of the present work is to investigate the acoustical properties of micro-capillary plates (MCP) in slip-flow regime characterized by holes diameters between 0.6 μm and 50 μm and a large perforation ratio, typically between 50 and 65%. The advantage of MCPs is to provide *ad-hoc* acoustic resistance and very low acoustic reactance over a broad frequency range, which is a key difference with respect to MPPs whose perforation ratio hardly exceed 10-15% and with holes diameter greater than 200 μm. In order to produce such small-sized holes, the photolithographic process, well-suited to produce MEMS (Micro-Electro Mechanical Sensors), has been used in bio-microfluidics to fabricate freestanding micro-perforated membranes made of solid polymer with holes diameter down to 10 µm [8]. This technology has been applied to fabricate silicon MPPs with minute holes diameters down to 27 µm and a perforation ratio up to 19%, thereby providing a bandwidth between 3 – 4 octaves with maximum absorption exceeding 0.85 [9].

In 1989, Dalmont *et al.* [10] studied the input impedance of a coupling cavity backed by a MCP with channel radius 12.5 µm in order to achieve a low-frequency anechoic termination of calibrated resistance for closed sound ducts in the no-flow case. Its suitable resistance value was obtained after minimizing the reflection coefficient of the coupling adapter assuming normal incidence and anechoic radiation load. A continuum model [11] was used for the MCP channels, although a slip-flow model would *a priori* be better suited for such small channels radius.

In the current study, one proposes a description of the MCP transfer impedance in slip-flow regime that goes beyond the continuum approach, e.g. down to channels radius of 0.6 µm. Moreover, an optimisation strategy is proposed based on minimising the acoustic power dissipated by the MCP. It is examined through modeling and experiments the acoustical performance of MCPs with near-optimal and non-optimal under a normal incidence plane wave.

Section 2 describes the physical characteristics of different MCPs and Section 3 presents an analytical model of the sound field propagation through MCPs in slip-flow regime. The simulated results are compared in Section 4 with measurements carried out in a Kundt tube for different configurations. Once the model has been verified, an optimisation study is presented in Section 5 for the physical MCP parameters affecting the performance of the device. Finally, we conclude with a summary of the main results and ideas for future work.

2. MCP MORPHOLOGY

MCPs are leaded glass plates comprising a large number of identical parallel channels, up to one million per cm², whose diameter d_0 ranges from 4 µm to 50 µm and thickness t from 0.5 mm to 5 mm so that the thickness-to-channel diameter ratio, t/d_0, is typically between 10 and 200.

MCP fabrication requires a glass tube fitted with a solid acid-etchable core material, repeatedly drawn and stacked to form an array of multi-fibers with the required diameter and filling fraction. The assembly is then fused to form a boule which is sliced to the required bias angle and thickness. Each slice is immersed in a chemical solution that dissolves the core fibers, leaving a glass plate with millions of micro-channels.

A photograph of a disk-shape Glass Capillary Array (GCA) is presented in Figure 1. Although it cannot be appreciated in the figure, GCA micro-channels are distributed in a triangular lattice, so that its perforation ratio, defined by $\sigma = 2\pi r_0^2 / \left(\sqrt{3}\, b^2\right)$, reaches 50% given a pitch (center-to-center channel spacing) $b = 33.7$ µm . Its micro-channels are straight tubes without bias angle and of constant cross-section so that the tortuosity factor is equal to one.

Table I shows the main physical parameters defining the two types of MCPs used in this study. For comparison purposes, these parameters are also presented for a classical MPP.

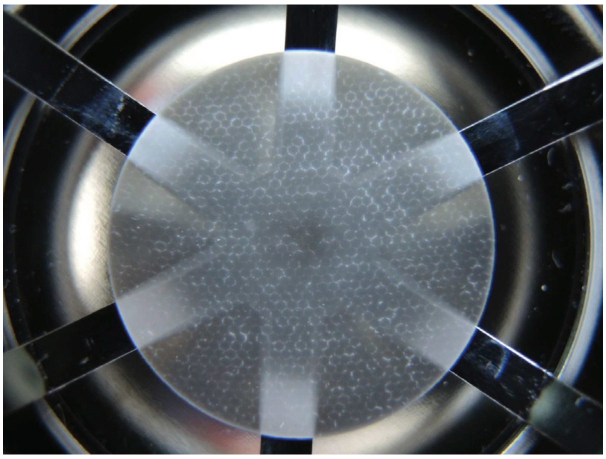

Figure 1. Photography of Glass Capillary Array I with outer diameter 25 mm.

Plate type	Channel radius (µm)	Knudsen number Kn	Perforation ratio (%)	Thickness (µm)	Aspect ratio	Number of channels per cm²
MPP	250	1.3×10^{-4}	0.79	500	1:1	4
MCP Glass Capillary Array I (GCA I)	12.5	5.1×10^{-3}	50	500	20:1	10^5
MCP Glass Capillary Array II (GCA II)	5	1.3×10^{-2}	68	2250	225:1	8.7×10^5

Table 1. Geometrical characteristics of MPP, GCA I, II and III; the aspect ratio is the thickness-to-channel diameter ratio, t/d_0, with $d_0 = 2r_0$, and the number of channels per cm² is $10^{-4}\sigma/\left(\pi r_0^2\right)$ with r_0 the channels diameter and σ the perforation ratio.

3. SLIP-FLOW MODELLING

The well-established continuous laws that have been used to study the propagation of sound through MPPs do not hold when addressing the problem with MCPs with holes diameters typically lower than 10 μm. This occurs when the holes radius r_0 approaches, even by several decades, the molecular mean free path Λ, the ratio Λ/r_0 defining the Knudsen number Kn [12, 13].

We first analyze in this section sound wave propagation through MCPs in slip-flow regimes, corresponding to $10^{-3} \le \mathrm{Kn} \le 10^{-1}$, or equivalently for $10\Lambda \le r_0 \le 1000\Lambda$. Slip-flow boundary conditions have first been derived [14, 15] in the frame of the kinetic theory of ideal monoatomic gases in contact with diffusively and specularly reflecting walls under isothermal condition. Performing a first-order Taylor expansion of these jumps as series of Kn leads to the following boundary conditions:

$$v_\Sigma = \frac{2-\sigma_v}{\sigma_v}\mathrm{Kn}\left.\frac{\partial v}{\partial n}\right|_\Sigma = B_v \left.\frac{\partial v}{\partial n}\right|_\Sigma , \quad (1)$$

$$\tau_\Sigma = \frac{2-\sigma_\tau}{\sigma_\tau}\frac{2\gamma}{\gamma+1}\frac{\mathrm{Kn}}{\mathrm{Pr}}\left.\frac{\partial \tau}{\partial n}\right|_\Sigma = B_\tau \left.\frac{\partial \tau}{\partial n}\right|_\Sigma , \quad (2)$$

satisfied by the trace on the channels wall surface Σ, of the axial particle velocity v and temperature disturbance τ as well as their normal derivative, $\partial/\partial n$, with respect to the dimensionless coordinate r/r_0 for a cylindrical channel, n being the unit normal entering the pore. In Eqns. (1,2), $\gamma = 1.402$ is the specific heat ratio, $\mathrm{Pr} = 0.71$ is the Prandtl number and σ_v (resp. σ_τ) is the fraction of molecules (resp. of their energy flux) reflected diffusively by the wall.

Assuming straight cylindrical channels with longitudinal axis z and harmonic regime ($e^{j\omega t}$), we apply linearized momentum and energy conservation to solve the momentum boundary-value problem (BVP) and transposing consequently the solution to the thermal BVP. The viscous transfer impedance of the channel, given per unit length is thus given by

$$Z_v = j\omega\rho_0 t\left\{1 - \frac{2}{k_v r_0}\frac{J_1(k_v r_0)}{\left[J_0(k_v r_0) - B_v k_v r_0 J_1(k_v r_0)\right]}\right\}^{-1}, \quad (3)$$

where $k_v = \sqrt{-j\omega\rho_0/\mu}$ is the viscous diffusion wavenumber and J_0 (resp. J_1) are the Bessel functions of the first kind of orders 0 (resp. 1). The overall transfer impedance of a MCP in the slip-flow regime can then be obtained as Z_v/σ. When $\mathrm{Kn} \le 10^{-3}$, it can be seen from Eqn. (1) that $B_v \approx 0$. Eqn. (3) reduces to the overall transfer impedance of a MPP in the continuum regime without pore end effects [1].

Analyzing the thermal BVP given by Eqn. (2), it can be seen that the solution is formally similar to Eqn. (3). The thermal transfer admittance of a channel, given per unit length, is given as follows

$$Y_\tau = \frac{j\omega}{\gamma p_0}\left\{1 + (\gamma-1)\frac{2}{k_\tau r_0}\frac{J_1(k_\tau r_0)}{\left[J_0(k_\tau r_0) - B_\tau k_\tau r_0 J_1(k_\tau r_0)\right]}\right\}, \quad (4)$$

with p_0 the ambient static pressure, $k_\tau = \sqrt{-j\omega\rho_0 C_p/\kappa} = k_v\sqrt{\mathrm{Pr}}$ the thermal diffusion wavenumber, C_p the specific heat capacity under constant pressure, κ the thermal conductivity coefficient, $\mathrm{Pr} = \mu C_p/\kappa$ the Prandtl number, μ the air dynamic viscosity and ρ_0 the air density. The effective or dynamic compressibility, $\chi_{\mathrm{eff.}}$, of a channel in the slip-flow regime, is then defined as $Y_\tau = j\omega\chi_{\mathrm{eff.}}$.

A common feature of the MCPs acoustical properties in both continuum and slip-flow regimes is their narrow channels behavior. It occurs if the channels Shear number $\mathrm{Sh} = r_0/\delta_{\mathrm{visc.}}$ is lower than unity, i.e. if the viscous boundary layer thickness, $\delta_{\mathrm{visc.}} = \sqrt{\mu/(\omega\rho_0)}$, exceeds the channels radius r_0. This occurs for frequencies up to $f_{\max} = \mu/\left(2\pi\rho_0 r_0^2\right)$, as it is met for GCA I and GCA II up to 7 kHz, the upper frequency range of the experiments presented in Section 4. As MCPs have narrow channel behavior, $|k_v r_0| < 1$, over a broad frequency range, we can perform Taylor series expansion of Eqns. (3) and (4) with respect to the Shear number $\mathrm{Sh} = |k_v r_0|$ up to order four. This leads to

$$Z_v \approx \frac{1}{1-4B_v}\left\{\frac{8t\mu}{r_0^2} + j\frac{4}{3}\omega\rho_0 t(1-6B_v)\right\}, \quad (5)$$

$$Y_\tau \approx \frac{j\omega}{p_0}\left\{1 - j\frac{(\gamma-1)}{8\gamma}\frac{C_p}{\kappa}\omega\rho_0 r_0^2(1-4B_\tau)\right\}, \quad (6)$$

which reduce, when $B_v = B_\tau = 0$, to Zwicker and Kosten low frequency approximation for the transfer impedance and admittance of narrow channels in continuum regime [11].

Assuming plane wave normal incidence, the amplitude reflection and transmission coefficients are defined as $r = (Z_1 - Z_0)/(Z_1 + Z_0)$ and $\tau = 2Z_0/(Z_1 + Z_0)$ with $Z_1 = Z_v/\sigma + Z_0$, the input impedance of the absorber backed by an anechoic termination, and $Z_0 = \rho_0 c_0$. The dissipation is then readily calculated as $\eta = 1 - |r|^2 - |\tau|^2$, the fraction of incident energy not reflected, nor transmitted. It is expressed in terms of $\alpha = 1 - |r|^2$ (resp. $t = |\tau|^2$) the energetic absorption (resp. transmission) coefficients.

Figure 2 shows the Knudsen number dependency of α, t and η for a 0.5 mm thick micro-perforate with a high density of holes ($\sigma = 50\,\%$, $b \approx 1.35 d_0$) when r_0 is decreased from 635 μm down to $10\Lambda =$ 0.64 μm while Kn increases accordingly.

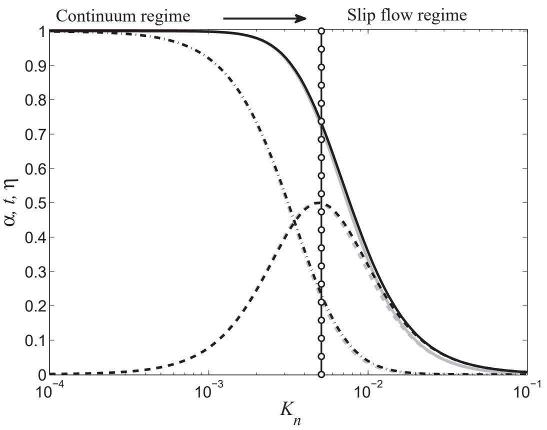

Figure 2. Knudsen number dependencies of the absorption (exact, ; approx.,), transmission (exact, ; approx.,) and dissipation (exact, ; approx,) coefficients of a MCP ($t = 0.5$ mm, $\sigma = 50\,\%$) assuming a slip-flow regime at 500 Hz; the vertical line with circles (-O-O-) corresponds to GCA I.

It can be seen that the narrow channel approximation given by Eqn. (5) well approximates the exact expression given by Eqn. (3) over a broad range of Knudsen numbers encompassing the continuum regime ($\mathrm{Kn} \leq 10^{-3}$). Although the continuum approach is not valid in slip-flow regime, it is found to be predictive of the MCP acoustical properties as long as $\mathrm{Sh} < 1$. For $\mathrm{Kn} \leq 10^{-3}$, almost all of the incident energy is transmitted by the highly porous MPP and is weakly dissipated. As the holes radius decreases, the transmission leakage decreases while back-reflection increases, but not at the same rate, so that part of the incident energy is dissipated within the MCP. A maximum of dissipation occurs in slip-flow regime that reaches $\eta_{\max} = 0.5$ for an optimal value of the holes radius $r_0^{\mathrm{opt}} = 12.8\,\mu\mathrm{m}$ ($\mathrm{Kn} = 0.005$). One observes from Table 1 and Fig. 2 that GCA I ($\mathrm{Kn} = 5.1 \times 10^{-3}$) is close to the optimal configuration.

Figures 3(a,b) show very distinct features between the MPP and the MCPs absorption properties, both in the unbacked and backed configurations. When unbacked, the MCPs exhibit flat absorption over the whole frequency bandwidth, that reaches $\alpha = 0.72$ for GCA I, whereas the MPP absorption falls above 200 Hz due to increasing back-reflections. When backed by a 5 cm depth cavity, the MPP provides narrowband absorption whose half-bandwith extends over one octave around the Helmholtz resonance with $\alpha_{\max} = 0.88$ at $f_{\mathrm{H}} = 629$ Hz. GCA I reaches similar maximum value $\alpha_{\max} = 0.85$, but provides a much broader absorption with a half-bandwidth that spans almost 9 octaves around $f_{\mathrm{H}} = 1668$ Hz. Given the same cavity depth, the increase of f_{H} from 629 Hz to 1668 Hz is due to a lower effective mass per unit area of GCA I with respect to the MPP. This is appreciated in Fig. 3(d) which shows that, unlike the MPP, the magnitude of the specific reactance, $\left|J_{\mathrm{tr}}/Z_0\right| \approx 4\omega t/(3\sigma c_0)$ [see Eqn. (5)], is almost zero-valued for the MCPs over a broad frequency range due to their high perforation ratio. Hence, from Eqn. (5), the overall MCP transfer impedance, Z_v/σ, then reduces to a pure resistance given by

$$R_{tr} \approx \frac{8t\mu}{\sigma r_0^2\left(1-4B_v\right)}, \tag{7}$$

that follows an inverse-power law of order 4 with respect to the channels radius and that does not depend on the frequency. This is illustrated in Fig. 3(c) in which it can be seen that GCA I input resistance is about $3.3\,\mathrm{Z}_0$, which is close to $3\mathrm{Z}_0$, the optimal input impedance (as shown in Sect. 5).

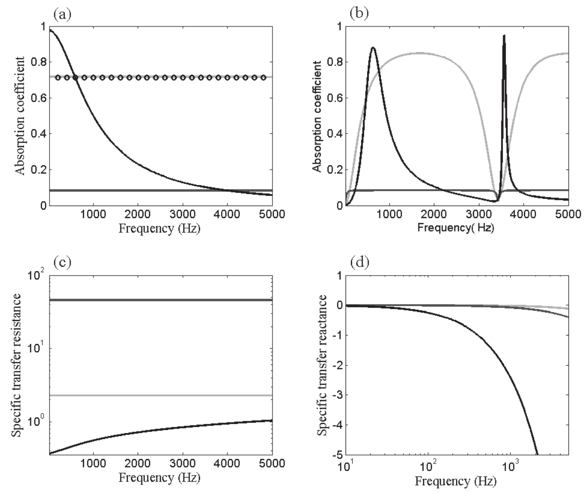

Figure 3. (a) Normal incidence absorption coefficients of unbacked MPP ( ), GCA I (exact, ; finite element, ○ ○), GCA II ( ) assuming anechoic load conditions; (b) Normal incidence absorption coefficients of rigidly-backed MPP ( ), GCA I ( ), GCA II ( ) with cavity depth $D = 0.05$ m; (c) Frequency dependence of the specific transfer resistance, R_{tr}/Z_0, related to MPP ( ), GCA I ( ), GCA II ( ); (d) Frequency dependence of the specific transfer reactance, J_{tr}/Z_0, related to MPP ( ), GCA I ( ), GCA II ( ).

4. EXPERIMENTAL STUDY

Validity of the model presented in the above section has been verified by a set of measurements in order to estimate the absorptive characteristics of the proposed MCPs described in Table I. A schematic of the physical set-up is presented in Fig. 4. A small impedance tube placed vertically has been installed in a semi-anechoic environment. This tube has dimensions of 80 cm-long with an inner radius $R = 1.5$ cm that provides a maximum frequency of analysis slightly less than 6700 Hz assuming plane wave regime. A random field is generated at one side of the tube for the determination of transfer function H_{12} between the acoustic pressures p_1 and p_2 measured by two 1/4" condenser microphones located upstream of the sample and separated by a distance $d = 5\,\text{cm}$, thus providing a lower frequency limit of 200 Hz for accurate measurements.

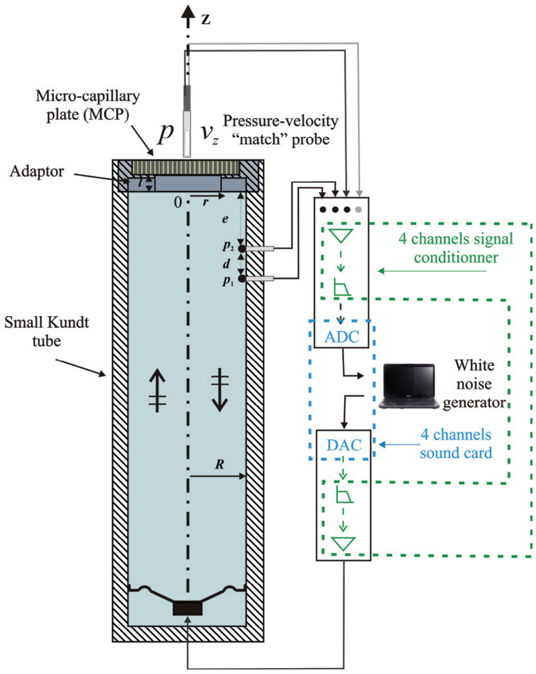

Figure 4. Schematic of the whole experimental set-up with cross-sectional view of the PVC circular adaptor into which the MCP was set.

Because the MCP has a radius of 1.275 cm that is smaller than the duct inner radius, it requires a thick PVC adaptor inserted into the tube and onto which the MCP is fixed, as shown in Figure 4. The adaptor introduces a constriction of radius $r = 1\,\text{cm}$ and thickness $l = 1\,\text{cm}$. Applying continuity of the pressures and acoustic flow rate at $z = 0$, one can estimate the MCP specific input impedance and its absorption coefficient. During the experiment, the output signals from the sensors were acquired using the OROS (type OR38) multi-channel system over a bandwidth 80 Hz – 6.7 kHz, at a sampling rate of 12.8 kHz and with a spectral resolution of 1.56 Hz, triggered on the generation of a white noise drive signal.

Figure 5(a) shows that plugging the thin GCA I disk onto the open tube termination, *via* the adaptor, significantly enhances the absorption coefficient over a broad bandwidth, as it reaches a constant value of 0.86 up to $k_0R = 0.3$ and then slowly decreases down to 0.7 up to $k_0R = 1.84$. This is appreciated when compared to the fraction of incident energy not reflected by the open adaptor which is minute below $k_0R = 0.4$ and that monotonically reaches a value of 0.65 towards $k_0R = 1.84$. One also observes in Fig. 5(a) that the theoretical model, which assumes plane wave anechoic load, provides a flat absorption spectrum that underestimates the measured absorption values by 20% up to $k_0R = 0.3$. Although not shown here, it was observed that the assumed load impedance behind the MCP has significant importance and should be, if possible, characterized before optimizing the MCP properties.

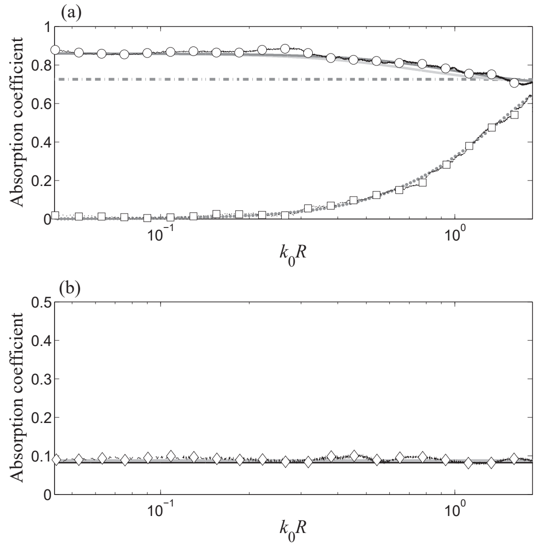

Figure 5. (a) Normal incidence absorption coefficients of unbacked GCA I: measured (-○-○-) and predicted assuming unflanged (▬▬), flanged (▬▬) and plane wave anechoic (▬ ▪ ▬) radiation conditions, and that of the open adaptor termination: measured (□┈□) and predicted assuming unflanged (●●●●) radiation condition; (b) Normal incidence absorption coefficient of unbacked GCA II: measured (◇--◇) and predicted assuming plane wave anechoic radiation condition (continuum regime, ▬▬; slip-flow regime, ▬▬).

5. OPTIMISATION

Optimization of the MPCs assuming a plane wave anechoic load is carried out in this section considering an unbacked MCP. It has been shown in Section 3 that the MCP input impedance $Z_1 = Z_v/\sigma + Z_0$ is well approximated by $R_{\text{tr}} + Z_0$ over a broad frequency range ($\text{Sh} < 1$) with R_{tr} given by Eqn. (7). An optimization study is now performed to find the optimal value of R_{tr} that maximizes the power dissipated by the MCP. The dissipation defined in Section 3 reads $\eta = 1 - \left(Z_R^2 + 4Z_0^2\right)/\left(Z_R + 2Z_0\right)^2$. It can be recast as a second-order equation in R_{tr},

$$\eta R_{\text{tr}}^2 - 4Z_0(1-\eta)R_{\text{tr}} + 4\eta Z_0^2 = 0, \tag{8}$$

the discriminant of which reads $\Delta = 16Z_0^2(1-2\eta)$. Eqn. (8) has real physical solutions if $\Delta \geq 0$, that is if $\eta \leq 1/2$. In other words, the dissipation of a single unbacked MCP with anechoic load cannot exceed 0.5, which was already observed in Fig. 2. In the case $\eta = \eta^{\text{opt}} = 1/2$ ($\Delta = 0$), the unique solution to Eqn. (8) is the optimal transfer resistance $R_{tr}^{opt} = 2Z_0$. The optimal channel radius that achieves maximum dissipation for a given perforation ratio can thus be obtained. For $t = 0.5$mm and $\sigma = 50\%$ (GCA I), this leads to $a^{opt} = 13.2\,\mu$m which is quite close to the actual value $12.5\,\mu$m for GCA I. Hence, GCA I is nearly optimal, as anticipated from Fig. 2, Fig. 3(a) and Fig. 5(a). For $t = 2.25$mm and $\sigma = 68\%$ linked to GCA II, this leads to $a^{opt} = 24\,\mu$m. This is much higher than the actual value $5\,\mu$m that provides too high resistance resulting in the low absorption values observed in Fig. 3(a) and Fig. 5(b).

One can deduce from $R_{tr}^{opt} = 2Z_0$ the optimal input impedance, absorption and transmission of MCPs under an anechoic load, namely $Z_1^{opt} = 3Z_0$, $\alpha^{opt} = 3/4$ and $\left|\tau^{opt}\right|^2 = 1/4$. Higher values of the absorption coefficient could be obtained for less resistive MCPs , described by the smallest of the two solutions to Eqn. (8), R_{tr}^{-}, with $R_{tr}^{\pm} = 2Z_0\left(1-\eta \pm \sqrt{1-2\eta}\right)\eta^{-1}$ assuming $\Delta > 0$ ($\eta < 1/2$). However, as it can be seen from the grey curves in Fig. 6, this would be at the expense of a lower dissipation and of a higher transmission. The black curves in Fig. 6 correspond to another class of MCPs with high resistance, low transmission and which reflect a large part of the incident wave.

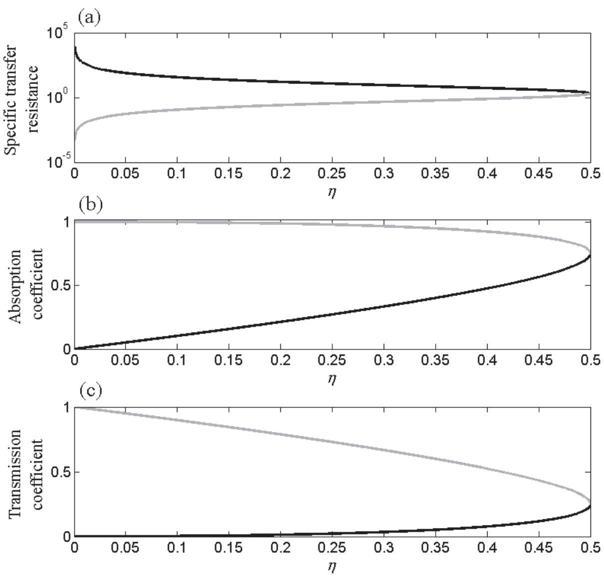

Figure 6. Dependence of (a) the specific transfer resistances $R_{tr}^{\pm}$, (b) the absorption coefficient and (c) the transmission coefficient to the power η dissipated by an unbacked MCP under an anechoic load.

6. CONCLUSIONS

In this work, a theoretical slip-flow model has been presented to estimate the efficiency of MCP absorbers to dissipate the power due to a normal incident plane wave. The model has been verified by a set of measurements performed in an impedance tube locaated in a semi-anechoic environment. The following points can be summarised from the results obtained:

- Because MCPs have a Knudsen number Kn usually comprised between 10^{-3} and 10^{-1}, their viscous transfer impedance and thermal admittance have been derived in the frame of the slip-flow regime. Theoretical modeling and FEM simulations showed that, in the broad frequency range over which MCPs exhibit narrow channel behaviour ($\mathrm{Sh} < 1$), the MCPs dissipation properties are well approximated by the continuum approach, up to a factor $\mathrm{Kn}\,\mathrm{Sh}^2$. Although not shown, It was found that the slip-flow model significantly deviates from the continuum approach when evaluating the transfer impedance of MCPs with extremely small channels radius, *e.g.* for $\mathrm{Kn} > 0.03$.
- Owing to their micrometric channels radius and high porosity, MCPs are pure resistive absorbers with constant resistance and minute reactance over a wide frequency band, the expression of which has been derived in terms of their constitutive parameters for $0.001 < \mathrm{Kn} < 0.1$. Theoretical and experimental studies showed the ability of unbacked optimal MCPs to achieve absorption values greater than 0.7 up to $k_0R = 1.84$ with a flat absorption plateau of 0.86 up to $k_0R = 0.3$ under normal incidence. MCPs could thus be used as suitably calibrated acoustic materials for low frequency anechoic terminations in the no-flow case.
- An optimization study has been performed of the MCPs dissipation properties under normal incidence angle and assuming anechoic radiation condition. It was shown that the optimal MCP resistance is given by $R_{tr}^{opt} = 2Z_0$ under an ideal anechoic load, leading to a maximum dissipated power of 0.5.

Ongoing works focus on the MCPs acoustical performance and the suitability of the continuum regime under a wide range of incidence angles for room acoustics applications. They also address the efficiency of rigidly-baked MCPs used as optimized locally-reacting wall treatments in flow ducts in order to ensure maximum damping of the principal duct mode.

7. ACKNOWLEGMENTS

This study was funded in Spain by the Ministerio de Economía y Competitividad project TRA2017-87978-R, AEI/FEDER, UE, and the mobility program ILINK+2018. It was supported in France by the ANR VIRTECH (ANR-17-CE10-0012-01). The authors would like to thank J. Kergomard, Emeritus Director of Research at CNRS-LMA, for fruitful discussions, Dr. P. Ecker from GIDS GmbH for kindly borrowing us one of the MCPs and Dr. L. Sabatier, Research Engineer at CNRS-LMA, for X-ray imaging the MCPs.

8. REFERENCES

[1] D. Y. Maa: "Potential of microperforated panel absorbers," *Journal of the Acoustical Society of America*, Vol. 104, pp. 2861–2866, 1998.

[2] D. Y. Maa: "Microperforated-panel wideband absorbers," *Noise Control Engineering Journal*, Vol. 29, pp. 77–84, 1987.

[3] T. Bravo, C. Maury and C. Pinhède: "Sound absorption and transmission through flexible micro-perforated panels backed by an air layer and a thin plate," *Journal of the Acoustical Society of America*, Vol. 131, pp. 3853–3863, 2012.

[4] T. Bravo, C. Maury and C. Pinhède: "Vibroacoustic properties of thin micro-perforated panel absorbers," *Journal of the Acoustical Society of America*, Vol. 132, pp. 789–798, 2012.

[5] K. Sakagami, Y. Nagayama, M. Morimoto and M. Yairi: "Pilot study on wideband sound absorber obtained by combination of two different microperforated panel (MPP) absorbers," *Acoustics, Science & Technology*, Vol. 30, pp. 154–156, 2009.

[6] Y. Li and B.M. Assouar: "Acoustic metasurface-based perfect absorber with deep subwavelength thickness," *Applied Physics Letters*, Vol. 108, No. 063502, 2016.

[7] M. Yang, S. Chen, C. Fu and P. Sheng: "Optimal sound-absorbing structures," *Material Horizons*, Vol. 4, pp. 673–680, 2017.

[8] Y. Zheng, W. Dai, D. Ryan and H. Wu: "Fabrication of freestanding microperforated membranes and their applications in microfluidics," *Biomicrofluidics*, Vol. 4, 036504, 2010.

[9] Y. J. Qian, D. Y. Kong, S. M. Liu, S. M. Sun and Z. Zhao: "Investigation on micro-perforated panel absorber with ultra-microperforations," *Applied Acoustics*, Vol. 74, pp.931–935, 2013.

[10] J.-P. Dalmont, J. Kergomard and X. Meynial: "Realization of an anechoic termination for sound ducts at low frequencies," *Comptes Rendus de l'Académie des Sciences*, Vol. 309 II, pp. 453–458, 1989 (text in French, includes abridged English version).

[11] C. Zwicker and C. W. Kosten: *Sound Absorbing Materials*, Elsevier Publishing Company, Inc., New-York, 1949 (reprinted by the Acoustical Society of the Netherlands, NAG).

[12] N. G. Hadjiconstantinou: "Sound wave propagation in transition-regime micro- and nanochannels," *Physics of Fluids*, Vol. 14, pp. 802–809, 2002.

[13] V. F. Kozlov, A. V. Fedorov and N. D. Malmuth: "Acoustic properties of rarefied gases inside pores of simple geometries," *Journal of the Acoustical Society of America*, Vol. 117, pp. 3402–3412, 2005.

[14] J. C. Maxwell: "On Stresses in Rarefied Gases Arising from Inequalities of Temperature," *Philosophical Transactions of the Royal Society Part I*, Vol. 170, pp.231–256, 1879.

[15] von M. Smoluchowski: "Ueber Wärmeleitung in verdünnten Gasen," *Annalen der Physik und Chemie*, Vol. 64, pp. 101–130, 1898.